JOURNAL OF MATERIALS SCIENCE 16 (1981) 2665–2674

Direct current arc-plasma synthesis of tungsten carbides

P. RONSHEIM, L. E. TOTH
Department of Chemical Engineering and Materials Science, University of Minnesota, Minneapolis, Minnesota, USA

A. MAZZA, E. PFENDER
Department of Mechanical Engineering, University of Minnesota, Minneapolis, Minnesota, USA

B. MITROFANOV
Ural Research Centre of the Academy of Science of the USSR, Institute of Chemistry, Sverdlovsk, USSR

Chemical reactions which occur in a thermal plasma between fine powders of tungsten and graphite and between powdered tungsten and methane have been studied. When using a commercial d.c. torch and a standard reactor design, the conversion to tungsten carbide is relatively poor. With a specially designed reactor operating in a transferred-arc mode, nearly complete conversion to carbide results when operating at the same power level and with methane as a reactant. Crystal structures and particle morphologies have been studied with electron microscopy and X-ray diffraction. Several initial stages of the particle–particle and particle–gas reactions have been determined. A number of interesting composite particles corresponding to intermediate reaction steps has been observed.

1. Introduction

There has been increasing interest in the use of plasmas for chemical synthesis of submicrometre refractory materials such as carbides, nitrides and borides. These materials are used as sintering additives, catalytic materials and dispersion strengtheners. Both r.f. and d.c. thermal arc-plasma techniques have been used in these developments, which have been principally exploratory. Results have shown that it is possible to prepare these powders when the reactants have been introduced in gaseous form, as a metal halide, for example [1–3]. One disadvantage of this method is that it is necessary to remove by-products such as HCl from the process.

A simpler method of injecting metallic powders directly into the plasma has generally not been successful. Recently, however, Canteloup and Mocellin [4] and Yoshida *et al.* [5] have directly synthesized refractory powders of silicon nitride and titanium nitride using an r.f. plasma. In this technique the metallic powders must vaporize completely and then react to form the products.

D.c arc-plasma synthesis with solid particle reactants is difficult because of two problems: (a) a plasma tends to reject the reactant particles before they enter the hot region, and (b) the residence time of the particles is not sufficient for complete evaporation and reaction [6]. Understanding and overcoming this problem would represent a significant advance in the general development of the plasma processing technique.

In this work, the preparation of tungsten carbide has been studied. This material has been chosen because tungsten has the highest melting point and graphite the highest sublimation point of the elements, and, therefore, success in this system would be particularly difficult while success in other system should be easier.

This report deals with two sets of experiments:

0022–2461/81/102665–10$03.00/0

a description of results from experiments using a commercial d.c. torch and a standard reactor and those describing the use of a reactor operating with an auxiliary anode. The first experiments deal with the injection of W and graphite powders into a standard type of reactor. Results show, however, that only a very small portion of W reacts. This is true even when the particle size of the injected powder is reduced to 1 to 2 μm. This particular phase of the present study is useful because it demonstrates several of the problems which are frequently encountered in either direct synthesis or direct reduction of materials. It is also useful because the complementary electron microscopy studies on the partially reacted products suggest some of the routes by which the reactions in the plasma are proceeding.

The second part describes the experiments and results using the auxiliary anode in basically the same reactor as before and operating at essentially the same power levels. Thus the two sets of experiments can be compared although several of the operating conditions are necessarily different. Experiments which investigate in more detail the operating conditions (temperature profiles, enthalpies, quench rates) of the transferred-arc mode are underway and details will be published elsewhere.

2. Experimental conditions

2.1. Arc-plasma reactor

The specially designed arc-plasma reactor with the auxiliary anode is shown in Fig. 1. Experiments with either the transferred or non-transferred arc could be conducted using the same reactor. The basic parts of the reactor are a conventional swirl-stabilized plasma torch, a reaction duct and a collection chamber. Reactants are injected in the plasma stream through an injection ring immediately downstream of the torch nozzle. Chemical reactions take place in the segmented 10 mm diameter graphite reaction tube whose length can be adjusted from 5 to 20 cm by adding or removing a number of graphite segments 2.5 cm long. The plasma torch is operated with argon in either the non-transferred or the transferred mode. In the non-transferred mode typical operating conditions are 450 to 500 A at 25 V. In the transferred mode an auxiliary water-cooled copper anode is inserted between the first and second segment of the reaction duct and a 150 A electric arc is maintained between the cathode of the plasma torch and this auxiliary anode with an overall applied voltage of about 50 V. The purpose of the transferred arc is to increase the temperature in the first section of the reaction duct in order to obtain better vaporization of the injected particles. Downstream of the anode the peak temperature of the plasma decays very quickly, from approximately 12000 K to 3000 K over a distance of about 2 cm, giving a rapid quenching to the reaction products. Further quenching can be obtained by radial injection of argon gas through the quenching ring located at the end of the reaction duct. Past this ring the quenched products enter the expanded volume of the cold-wall collection chamber.

The initial transferred arc design used a graphite tube between the first and second anode. The injected powders accumulated at the cold auxiliary anode and shorted out the arc along the graphite tube. Use of a boron nitride reaction tube in the transferred arc region eliminates this difficulty. The arc voltage remains steady over the time of the run. Little boron nitride erosion occurs except at the anode edge where the arc attaches.

The starting materials for the carbide production are 99.9% tungsten powders (1–2, 8–12, 12–25 μm) from Cerac, spectroscopic-grade graphite powders (<325 and <200 mesh) from Alfa, and ultra-high purity methane from Matheson Gas Products. After these materials have passed through the plasma reactor, the products are brushed from the walls of the collection chamber and analysed by X-ray and electron microscopy techniques.

2.2. Materials analysis

Phases present in the collected powders are identified with a Siemens X-ray diffractometer. The diffractometer data are also used to obtain a semi-quantitative measure of the carbide production. Intensities of selected diffraction peaks from each phase are determined by measuring the areas under the diffraction peaks. These intensities are then adjusted to determine relative amounts of each phase present by introducing the structure and multiplicity factors, the absorption coefficient and Lorentz polarization factor for the angle at which the peak is found. The structure factor being used for the carbides includes the carbon lattice contribution, although the tungsten provides most of the diffracted intensities.

A JEOL Co. 100 CX electron microscope

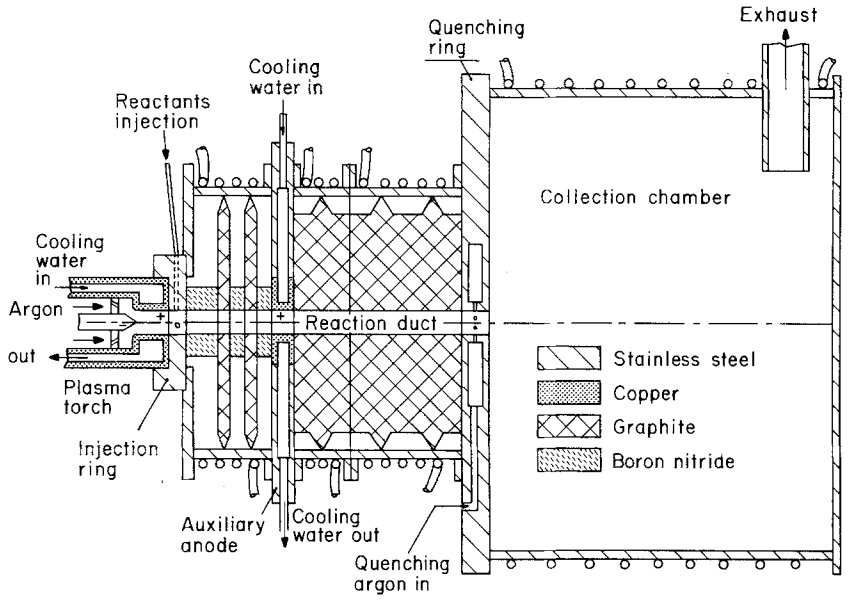

Figure 1 Schematic diagram of the experimental reactor.

(STEM) operated at 100 kV is used to observe the particles. Samples are prepared for electron microscopy by first dispersing the powder in a soapy water suspension. A small drop of the suspension is allowed to dry on a copper grid coated with Formvar and evaporated carbon. A 10 nm gold film is also evaporated on to the grid to allow accurate camera constant determination for electron diffraction.

3. Experimental results

3.1. Standard reactor design non-transferred arc

In the standard design the powders are injected into the tail end of the plasma just below the torch anode. The graphite and tungsten powders are injected simultaneously through different ports located at 180° apart. Operating conditions for the various runs are listed in Table I which

TABLE I Experimental conditions and products for runs with W and graphite or methane reactants in standard reactor design

Sample number	Particle injection		Power input torch	Torch flow ($dm^3 min^{-1}$)	Quench flow ($dm^3 min^{-1}$)	Carbide production (at% W)			
	Tungsten	Graphite				W	W_2C	α-WC	β-WC
101	8–12 μm 5 g min^{-1}	–74 μm 1.2 g min^{-1}	450 A 26 V	11	11	79	21	–	–
102	8–12 μm 5 g min^{-1}	–74 μm 1.2 g min^{-1}	450 A 26 V	11	11	97	3	–	–
103	8–12 μm 3–4 g min^{-1}	–74 μm 1.2 g min^{-1}	500 A 26 V	11	5.6	95	4	–	1
113	1–2 μm 0.5 g min^{-1}	–44 μm 1.0 g min^{-1}	450 A 25 V	11	–	45	51	–	4
104	8–12 μm 3–4 g min^{-1}	methane	500 A 25 V	11	5.6	72	28	–	–
105	8–12 μm 3–4 g min^{-1}	methane	450 A 25 V	11	5.6	63	37	–	–
106	8–12 μm 3–4 g min^{-1}	methane	450 A 25 V	11	11.2	82	18	–	–
111	1–2 μm 0.5 g min^{-1}	methane	450 A 25 V	11	5.6	36	50	6	9
112	1–2 μm 0.5 g min^{-1}	methane	450 A 25 V	11	5.6	51	38	5	6

includes injection rates for particles, voltage and current conditions of the torch, the Ar flow rate through the torch and quenching gas flow rates. In this mode of operation about half of the total power to the torch is dissipated in heating the cooling water passing through the anode and the remaining power is available to heat the injected particles. Table I also lists the products as determined by X-ray analysis and electron microscopy. The number in the table corresponds to percentages of each phase given in atomic per cent W. Any excess carbon or graphite present in the products is not included in the percentages.

In the first runs, 101 to 103, when 8 to 12 μm W and $< 74\,\mu$m graphite powders are injected into the plasma, very little of the W is converted to a carbide. Both X-ray and electron microscopy analyses show that nearly all W and graphite passes through the reactor unaltered and unreacted. For example, the X-ray patterns of the products all show sharp diffraction peaks for tungsten. These lines have very nearly the same line-shape and width as the patterns of the W starting powders. Since peak widths are a measure of the particle size (the broader a diffraction peak the smaller the particle size), the similarity of the patterns indicates that the W is passing unaltered through the plasma. Likewise, the X-rays of the products show a strong (0 0 2) diffraction peak for graphite at a d-spacing of 0.335 nm. X-rays of the starting graphite powders also show that the (0 0 2) peak at 0.335 nm is the most intense one in the spectrum.

An electron microscopy analysis of the products shows that the shape and size of the tungsten and graphite powders from Runs 101 to 103 are comparable to those of the starting materials. This result indicates that either the particles do not successfully penetrate the plasma or that their residence time is insufficient to allow them to vaporize completely. Electron microscopy shows, however, that the surfaces of these particles are spotted with a carbide material. These particles are W_2C and have a 1 to 30 nm diameter range.

The lattice parameters for W_2C are $a = 0.2994$ nm and $c = 0.4712$ nm, in good agreement with literature results. A small amount of β-WC is observed in the electron microscopy studies of one sample. More details of the microscope studies will be given later.

When it was realized that the injected particles were not being evaporated in the plasma, it was decided to reduce the particle sizes of both starting materials in an attempt to improve conversion. The powder sizes, 1 to 2 μm for W and $< 44\,\mu$m for graphite, are the smallest readily available commercially. The conversion to carbide did improve dramatically (Table I, Run 113). Yet analysis of the products shows that much of the W and graphite still are not being evaporated.

Changing the carbon source from graphite to methane also improves the conversion rate, as can be seen in Table I. The main products are unreacted W (for both the 8–12 μm and 1–2 μm cases), W_2C and amorphous carbon. Reducing the particle size of W to 1 to 2 μm increases the conversion rate to carbides, mainly W_2C, and also produces some α- and β-WC.

Electron microscopy also shows large quantities of unreacted amorphous carbon with a particle size of 5 to 10 nm. The W_2C particles are found in clusters. The individual particles within the clusters are 25 to 30 nm with little variation in size. Some particles exhibit hexagonal, and others cubic, symmetry.

This set of experiments shows that it has not been possible to react completely injected particles of W and graphite or even W and methane with the conventionally designed plasma reactor and the available power. The experiments do indicate that a power increase could lead to full conversion. No such attempt was made since the torch and reactor were not designed for higher power levels.

3.2. Transferred arc

In the transferred arc mode of operation, a plasma is first established in the torch and then transferred to the auxiliary anode, leaving the torch anode at a floating potential. A major advantage of this design is that powders are injected into a current-carrying plasma rather than at the tail end of a field-free plasma. In the present design, powders are injected at the same location as used in the standard reactor design, or 3.5 cm upstream from the auxiliary anode. Particles thus have a longer residence time in the plasma to react. Carbon tends to deposit in the reaction tube as graphite, constricting the tube and changing the flame characteristics. To minimize this problem the argon flow rate through the torch is increased to about 18 $dm^3\,min^{-1}$ from a previous value of 11 $dm^3\,min^{-1}$. Particles, therefore, move faster

TABLE II Experimental conditions and products for runs with W and graphite as reactants and with the transferred arc

Sample number	Particle injection		Power input		Torch flow ($dm^3 min^{-1}$)	Quench flow ($dm^3 min^{-1}$)	Carbide production (at% W)			
	Tungsten	Graphite	Torch anode	Transfer anode			W	W_2C	α-WC	β-WC
120	1–2 μm	–44 μm	200 A	125 A	9.4	11	20	80	–	–
	0.5 g min^{-1}	1.0 g min^{-1}	16 V	45 V						
126	1–2 μm	–44 μm	150 A	150 A	18.8	11	76	16	7	1
	0.5 g min^{-1}	1.0 g min^{-1}	20 V	55 V						
127	1–2 μm	–44 μm	150 A	150 A	18.8	11	14	51	3	33
	0.5 g min^{-1}	1.0 g min^{-1}	20 V	55 V						

through the reaction zone, offsetting some of the advantage gained from the longer arc. A few runs have been made with a lower torch flow rate but could not be continued for longer then ten minutes due to carbon deposition.

Four sets of data are presented here illustrating the use of the reactor with the transferred arc: (a) 1 to 2 μm tungsten with < 44 μm graphite, (b) 1 to 2 μm W with methane in a W:C atomic ratio of 1:10, (c) 1 to 2 μm tungsten and methane with a reduced W:C ratio in an attempt to produce W_2C, and (d) a gas–gas reaction between WCl_6 and CH_4. These experiments will now be discussed in order.

3.2.1. Transferred arc: W and graphite reactants

In runs with injected W and graphite powders, the amount of injected carbon is about thirty times that required to produce WC. The phases present in the products are W, W_2C, β-WC, α-WC and graphite (see Table II). Results show that the conversion to carbide is not complete and that only a small fraction of the available carbon is used for carbide formation. Averaging the results of Runs 120, 126 and 127 it can be seen that the major phase is W_2C. One sample, 127, contains appreciable quantities of β-WC.

While not evident from Table II, details of the electron microscopy and X-ray analysis show significant changes in the materials from that found in all runs with the standard reactor design. For example, in all transferred arc runs, the X-ray diffraction peaks for the plasma-processed graphite are different from those for the starting graphite powder. The (1 0 1) peak has shifted to $d = 0.205$ nm from 0.203 nm and the intensity of this peak is now greater than for the (0 0 2) peak. There is considerable line-broadening of all peaks indicating a fine particle size for graphite.

Electron microscopy studies confirm these results and show directly that the injected graphite and nearly all W powders have been disintegrated or evaporated by the plasma. The graphite is now in the form of small thin flakes about 10 nm thick. The graphite contains many dispered W_2C or α-WC particles. This type of composite particle will be discussed later. There is also some amorphous carbon in the deposits, but no indication of the relatively large injected graphite particles. In addition to the W_2C dispersed in the graphite sheets, there are separate clusters of W_2C. Sample 127 also contains appreciable quantities of β-WC. Much of the unreacted W is predominantly in the form of 10 to 20 nm particles and only a few large micrometre-sized particles are seen. When W is injected alone into the reactor the product is predominantly 10 nm-sized powder, as determined by electron microscopy.

3.2.2. Transferred arc: W and methane reactants

Results of runs with 1 to 2 μm W and methane in the atomic ration W:C of 1:10 are shown in Table III. The purpose of these runs is to determine if WC can be produced without also producing subcarbides. Because the powder feeder is not perfectly calibrated and did not operate uniformly over extended periods of time, the exact W:C ratio may vary from run to run. Comparison of Runs 121 and 128 give some indication of the uncertainty.

The principal phase in all runs is β-WC. Fig. 2 shows a trace of the X-ray diffraction pattern for one sample in which the product is 96% β-WC. The average amount of β-WC (and α-WC) in the four samples is 85%. There are also minor amounts of W ($\sim$ 8%) and W_2C ($\sim$ 7%). Electron microscopy shows the presence of some unreacted amorphous carbon in the products and some unreacted tungsten. There is no detectable graphite in the

TABLE III Experimental conditions and products for runs with W and methane in a W:C ratio of 1:10 and with a transferred arc

Sample number	Particle injection: tungsten	Power input		Torch flow ($dm^3 min^{-1}$)	Quench flow ($dm^3 min^{-1}$)	Carbide production (at% W)			
		Torch	Transfer			W	W_2C	α-WC	β-WC
121	1–2 μm	200 A	125 A	9.4	–	6	11	3	80
	0.3 g min^{-1}	16 V	45 V						
122	1–2 μm	150 A	150 A	18.6	11.2	16	5	5	74
	0.3 g min^{-1}	20 V	55 A						
128	1–2 μm	150 A	150 A	9.4	–	2	2	–	96
	0.3 g min^{-1}	20 V	55 V						
129	1–2 μm	150 A	200 A	18.6	–	9	8	5	78
	0.3 g min^{-1}	20 V	55 V						

products. Surprisingly, the run in which a quench is introduced has the smallest conversion to β-WC. The probable reason for this is that the quench extinguishes the plasma rather abruptly and also terminates the reaction. Since in all runs only a small amount of α-WC is produced compared to β-WC, the natural quench rate is sufficient to stabilize the high-temperature β-WC phase.

The β-WC from these runs has the B1 crystal structure with $a = 0.4229$ nm. This compares to a lattice parameter of $a = 0.4220$ nm determined by Rudy *et al.* [8] for β-$WC_{0.61}$ and this indicates that the present β-WC may contain a higher carbon content. Particles sizes, determined by electron microscopy, range from 2 to 16 nm. Individual carbide particles are often agglomerated into large clusters. These can be easily dispersed with the soapy solution used to prepare the specimens for examination. No graphite, or composite particles of graphite and W_2C, is found, and very little physically unaffected W is observed. The unreacted W particles are about 10 nm in size.

Several runs have been made in which the W:C ratio has been reduced in an attempt to produce single-phase W_2C. The results are given in Table IV. In three runs, roughly equal amounts of W, W_2C and WC are produced, the ratios being, $W:W_2C:WC = 30:32:38$. Thus, it is clear that the reaction proceeds too inhomogeneously to produce the subcarbide in a pure state.

To understand better the reaction process, one experiment has been carried out using the gas–gas reaction, WCl_6 and methane, introduced into the reactor in a W:C ratio of about 1:1. The amount of WCl_6 introduced into the reactor has been determined by monitoring the temperature of a

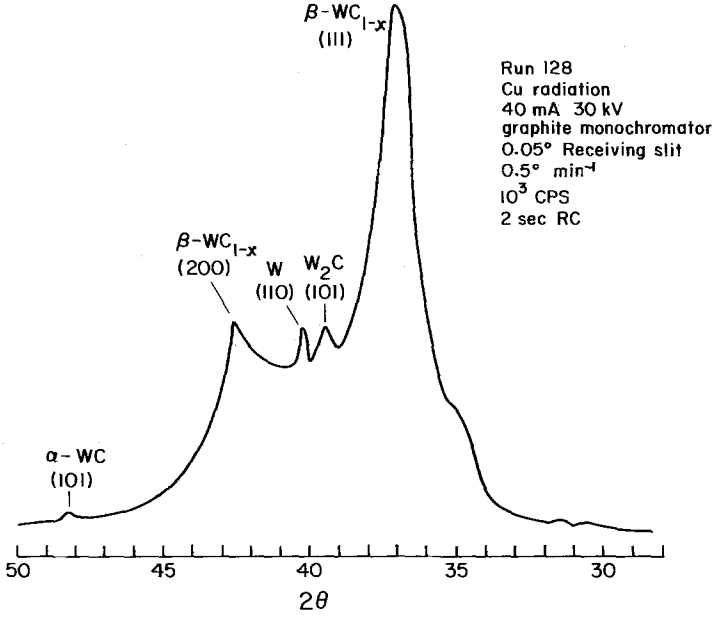

Figure 2 X-ray diffractometer chart for Run 128.

TABLE IV Experimental conditions and products for runs with W and methane in a W:C ratio near 1:1 and with a transferred arc

Sample number	Particle injection	Power input		Torch flow ($dm^3 min^{-1}$)	Quench flow ($dm^3 min^{-1}$)	Carbide production (at% W)			
		Torch anode	Auxiliary anode			W	W_2C	α-WC	β-WC
123	1–2 μm 0.3 g min^{-1}	150 A 20 V	150 A 55 V	18.6	11.2	15	29	16	40
124	1–2 μm 0.3 g min^{-1}	150 A 20 V	150 A 55 V	18.6	11.2	27	48	9	16
125	1–2 μm 0.3 g min^{-1}	150 A 20 V	150 A 55 V	18.6	–	47	18	12	23

WCl_6 cell and using the known thermodynamic data [9] for the vapour pressure of WCl_6. Results show that only W_2C and β-WC are produced and these occurred in the ratio of about 35:65. A large carbon excess is not required for complete reaction of the gas-phase reactants. Thus it is clear that it is far easier to control gas–gas reactions than solid–solid or solid–gas reactions in which a large excess of carbon is required for complete reaction. The significance of this experiment will be discussed later.

4. Reaction mechanisms and electron microscopy

Results of electron microscopy and X-ray diffraction show that the reactions leading to carbide production depend on both the reactor design and the injected materials. In the standard reactor design with the nontransferred arc, the reactions are characterized as being incomplete whereas with the transferred arc the reactions are more nearly complete, but depend on whether graphite or methane is injected.

A detailed analysis has been performed on Sample 103 which was produced from graphite and W with a non-transferred arc. Fig. 3 is a low magnification photograph of the products showing the nearly unaffected round tungsten particles and the irregularly-shaped graphite particles. Closer inspection of the graphite particles reveals dark W_2C particles dispersed on thin graphite sheets. Either the tungsten condenses and reacts on the graphite or vaporized carbon and tungsten condense together on the graphite particle. Fig. 4 shows W_2C particles (dark) formed within a larger graphite particle (light). The figure also shows Moiré patterns which indicate that one or more graphite sheets, about 10 nm thick, are on top of one another. Fig. 5 shows a selected-area electron diffraction pattern of this composite particle with double diffraction effects due to the overlapping particles. The results shown in Figs 4 and 5 might be expected if the graphite was in the process of breaking up in the intense heat of the plasma. In other words, the graphite is exfoliating along the (0 0 2) planes and at the same time reacting to

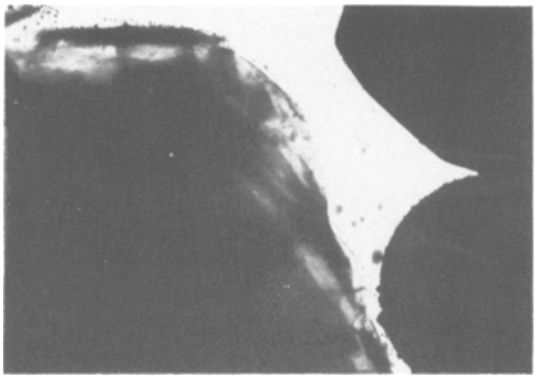

Figure 3 TEM photograph of poorly vaporized W and graphite. The larger irregularly-shaped object is graphite; the rounder, denser objects are tungsten. Sample 103. × 4200.

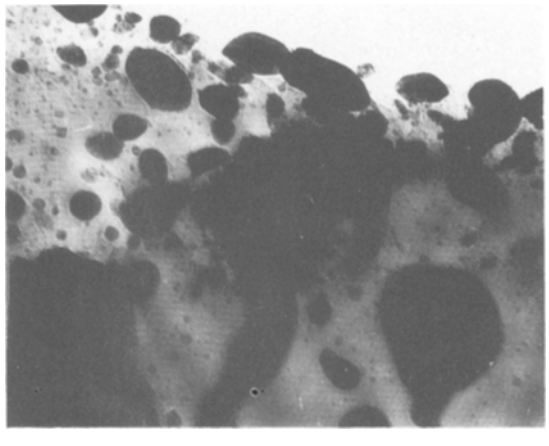

Figure 4 Close-up of W_2C particles in graphite. The parallel lines are Moiré patterns. Sample 103. × 160 000.

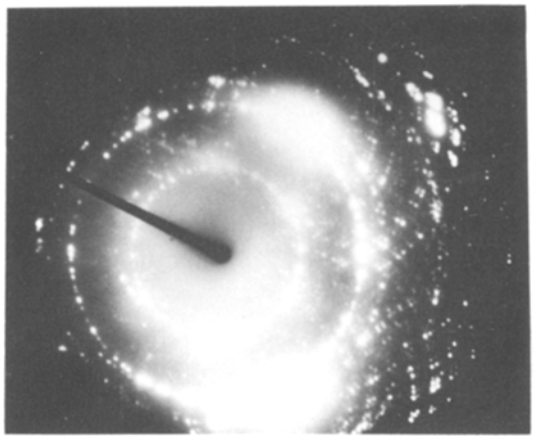

Figure 5 Small-angle X-ray diffraction pattern from graphite sheets. Double diffraction due to overlying crystals is seen in the secondary ring patterns centred on the (1 1 0) line of the primary rings. Sample 103.

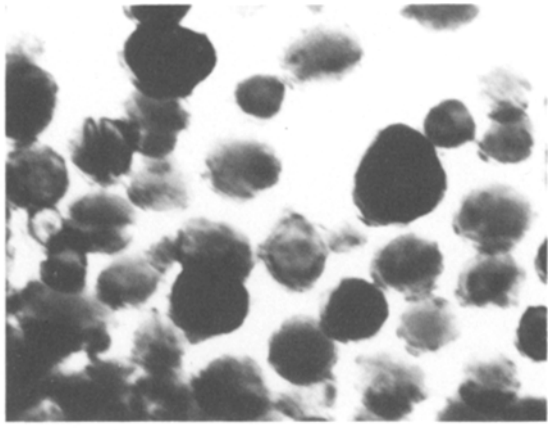

Figure 7 β-WC_{1-x} particles. The concentric rings in the particles are due to thickness produced phase interference. The bisecting bands are caused by lattice-plane interaction with the electron beam. Sample 103. × 123 000.

form W_2C. Because this formation occurs at the graphite, the W must have evaporated and condensed at the graphite and not vice versa. Fig. 6 is a high resolution SEM photograph showing that the W_2C is not uniformly distributed in the graphite. Tungsten is a strong emitter of secondary electrons compared to graphite and the W_2C particles appear bright in the photograph. The particles tend to be concentrated in clusters along the perimeter. The similarity of the hexagonal carbon lattice in W_2C and the graphite would explain the association of W_2C rather than the cubic β-WC with the graphite sheets. Fig. 7 shows some particles of β-WC which also formed in Sample 103; their presence in the sample illustrates the non-uniform nature of the reaction. The β-WC is found separated from the graphite flakes.

It is clear from the detailed analysis of Sample 103, that the overall conversion to carbide is incomplete and that several steps are simultaneously occurring: evaporation of W, formation of W_2C at graphite, exfoliation of graphite and condensation of β-WC.

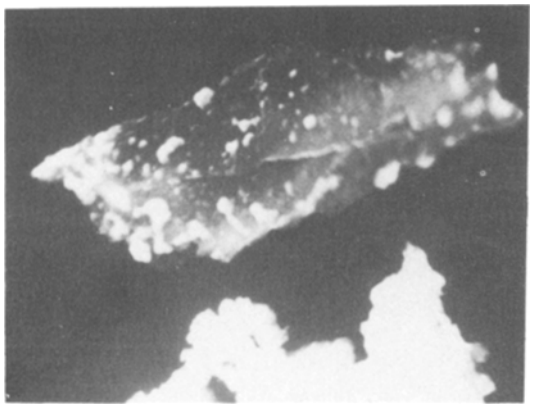

Figure 6 SEM micrograph of a structure similar to that of Fig. 4. The bright particles are W_2C. Sample 103. × 6500.

Detailed microscopy has also been performed on Sample 120, which is typical of runs in which 1 to 2 μm W and graphite are injected into a transferred-arc plasma. It is evident from the microscopy that the reaction has proceeded further than in Sample 103, discussed above. The large graphite particles have disappeared and most of the W is vaporized. An interesting new type of composite particle is found in abundance (Fig. 8). These are very thin sheets (10–20 nm) of graphite with W_2C or α-WC particles dispersed in them. These particles are similar to those found in Sample 103, but now it appears that the exfoliation is complete so that the graphite sheets are separate from one another. Another possible, although less likely explanation, is that the particles grew by simultaneous condensation of W and C. Whereas W_2C and α-WC are found associated with graphite, β-WC particles are again found in isolated clusters.

When methane is used as a reactant and the transferred arc is still employed, there is an increase in the amount of β-WC produced (more complete reaction). These β-WC particles are found with excess amorphous carbon (see Fig. 9). In Runs 121, 122, 138 and 129 where 85% or more of the product is β-WC, it is not possible to distinguish the individual particles of W_2C and W from β-WC as all particles are agglomerated into large clusters.

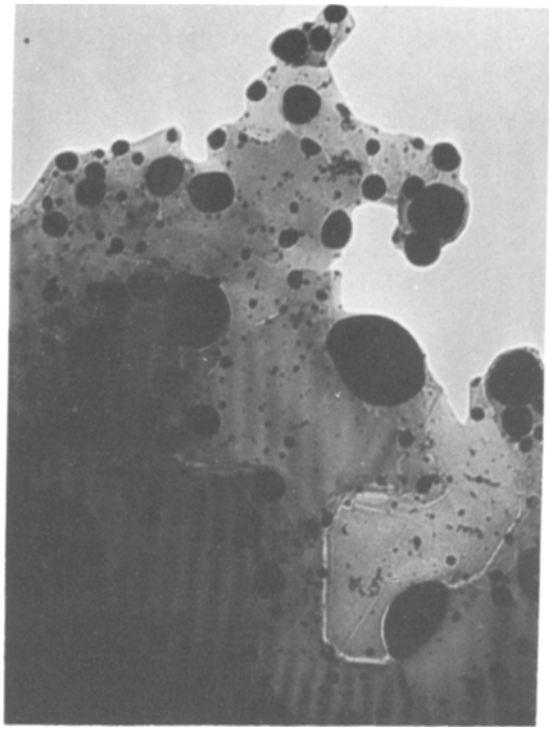

Figure 8 TEM micrograph of the graphite–W_2C structure. × 160 000.

In marked contrast are the results when tungsten hexachloride and methane are the reactants. The reaction is complete and uniform with β-WC and W_2C forming in approximately the proper ratios and with no W in the product. There is a small amount of unreacted carbon present in the sample. This is very different from the large carbon excess required for complete reaction of the solid particle reactants. This difference in behaviour can be explained in the following manner. The WCl_6 and CH_4 require less energy to dissociate than is required to heat and vaporize W or graphite particles. In the former case, the dissociated W and C atoms reach a higher temperature and, presumably, more active state. Thus, the carbide-formation reaction proceeds more readily. With solid–solid or solid–gas reactants, not all the solid particles are completely evaporated and part of the reaction occurs by carburization. Unsuccessful attempts to form WC from W and methane are a good illustration of the non-uniformity of the latter reactions.

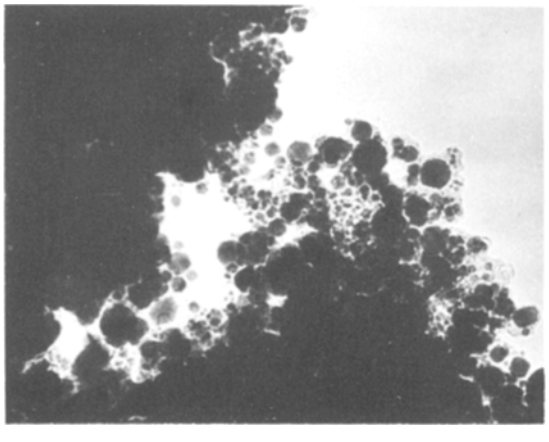

Figure 9 β-WC_{1-x} crystals with nearly electron-transparent carbon. Sample 121. × 335 000.

5. Summary

The reactor design used in this work is successful in introducing the solid particle reactants into the plasma. Analyses indicate that the major obstacle to full reaction is providing sufficient power and residence time in the plasma for the particles to vaporize and reach the required reaction temperature. The use of the transferred arc clearly increases the overall reactivity of the particles while using no more power than the conventional plasma torch design.

Acknowledgements

This work has been supported by the National Science Foundation NSF/ENG 78-10047. The authors wish to thank Paul Blaske and Beth Davidian for their technical assistance and the Space Science Center at the University of Minnesota for the grant for use of the electron microscopy facilities.

References

1. H. HARNISH, G. HEYMER and E. SCHALLUS, *Chem. Ing. Tech.* **35** (1963) 7.
2. E. NEUENSCHWANDER, *J. Less-Common Metals* **11** (1966) 365.
3. P. H. WILKS and D. R. LACROIX, Proceedings of the Electrochemical Society Fine Particles Symposium, October 1973, Boston (John Wiley and Sons, New York, 1974) pp. 180–6.
4. J. CANTELOUP and A. MOCELLIN, "Special Ceramics", Vol. 6, edited by P. Popper (British Ceramic Research Association, Stoke-on-Trent, 1975).
5. T. YOSHIDA, A. KAWASAKI, K. NAKAYAWA and K. AKASHI, *J. Mater. Sci.* **14** (1979) 1624.
6. C. SHEER, S. KORMAN, D. J. ANGIER and R. P. CAHN, Proceedings of the Electrochemical Society Fine Particles Symposium, October 1973, Boston, (John Wiley and Sons, New York, 1974) pp. 133–147.
7. L. E. MURR, "Electron Optical Applications in

Materials Science", (McGraw-Hill, New York, 1970) p. 402.
8. E. RUDY, S. WINDISH and J. R. HOFFMAN, Air Force Materials Lab., *AMFL-TR-65-2,* Part 1, Vol. VI, (1966).
9. F. D. STEVENSON, C. E. WICKS and F. E. BLOCK, US Bureau of Mines Report on Investigation No. 6362(2) (1964).

Received 17 September and accepted 13 October 1980.